

Bandwidth control in a perovskite-type $3d^1$ -correlated metal $\text{Ca}_{1-x}\text{Sr}_x\text{VO}_3$.

II. Optical spectroscopy

H. Makino

Institute of Applied Physics, University of Tsukuba, Tsukuba 305, Japan

I. H. Inoue*

PRESTO Japan Science and Technology Corporation, and Electrotechnical Laboratory, Tsukuba 305, Japan

M. J. Rozenberg

Institut Laue Langevin, Boîte Postale 156X, 38042 Grenoble Cédex 9, France

I. Hase and Y. Aiura

Electrotechnical Laboratory, Tsukuba 305, Japan

S. Onari

Institute of Applied Physics, University of Tsukuba, Tsukuba 305, Japan

(Received 29 December 1997)

Optical conductivity spectra of single crystals of the perovskite-type $3d^1$ metallic alloy system $\text{Ca}_{1-x}\text{Sr}_x\text{VO}_3$ have been studied to elucidate how the electronic behavior depends on the strength of the electron correlation without changing the nominal number of electrons. The reflectivity measurements were made at room temperature between 0.05 eV and 40 eV. The effective mass deduced by the analysis of the Drude-like contribution to the optical conductivity and the plasma frequency do not show critical enhancement, even though the system is close to the Mott transition. Besides the Drude-like contribution, two anomalous features were observed in the optical conductivity spectra of the intraband transition within the $3d$ band. These features can be assigned to transitions involving the incoherent and coherent bands near the Fermi level. The large spectral weight redistribution in this system, however, does not involve a large mass enhancement. [S0163-1829(98)03332-3]

I. INTRODUCTION

Over the past few decades, a considerable number of studies have been performed on $3d$ transition-metal oxides that have a considerably narrow $3d$ band. In particular, a metal-to-insulator transition caused by a strong electron correlation¹ (Mott transition) as well as anomalous electronic properties in the metallic phase near the Mott transition have attracted the interest of many researchers. Since the discovery of the high- T_c cuprate superconductors, the importance of two types of experimental approaches to the Mott transition have been discussed intensively: a filling control and a bandwidth control. The former consists of doping holes or electrons to the system, and the latter of varying the strength of the electron correlation U/W , where U is the electron correlation due to Coulomb repulsion and W is the one-electron bandwidth.

In recent years, the systematic evolutions of optical conductivity spectra in going from a correlated metallic phase to the Mott-Hubbard insulating phase have been reported on both the filling-controlled²⁻⁶ and the bandwidth-controlled Mott-Hubbard systems.⁷⁻¹⁰ The smallest energy gap for charge excitations of the Mott-Hubbard insulator is the excitation energy of the charge fluctuation $d^n + d^n \rightarrow d^{n-1} + d^{n+1}$, so-called a Mott-Hubbard gap.¹¹ The optical conductivity of the Mott-Hubbard insulator is considered to show a gap feature due to the above charge excitation from the lower Hubbard band to the upper Hubbard band.

V_2O_3 and related compounds have been extensively studied as typical materials that show the Mott transition with varying the strength of the U/W ratio. The temperature dependent optical conductivity of V_2O_3 was reported by Thomas *et al.* through the metal-to-insulator transition.^{9,10} The optical conductivity of V_2O_3 in the insulating phase shows a gap feature, which is attributed to the Mott-Hubbard gap excitation. On the other hand, in the metallic state, a low-energy contribution to the optical conductivity shows an anomalous feature, which is reproduced by two Lorentzians. Moreover, the optical conductivity shows an anomalous enhancement of the spectral weight as a function of temperature. Rozenberg *et al.* reported that these experimental results are in good agreement with the theoretical prediction obtained by the infinite-dimension Hubbard model within the mean-field approach.¹⁰ Since the formation of the Mott-Hubbard bands are predicted even in the metallic state for this kind of strongly correlated system, the optical conductivity spectra should be affected by the precursor features.¹² It is very interesting to see how the spectral weight varies with the electron correlation in the correlated metallic state near the Mott transition. For a detailed discussion, however, we need to control the strength of the electron correlation more precisely.

The perovskite-type early $3d$ transition-metal oxides are ideal Mott-Hubbard systems for controlling the band filling and bandwidth by chemical substitutions. It has been reported that, for the filling controlled systems $\text{La}_{1-x}\text{Sr}_x\text{TiO}_3$

and $R_{1-x}\text{Ca}_x\text{TiO}_3$ (R =rare earth), the spectral weight of the optical conductivity transfers from the higher-energy feature corresponding to an excitation through the Mott-Hubbard gap, to the midinfrared inner-gap region corresponding to the Drude-like absorption extending from $\omega = 0$.^{2,3,6} The rate of the spectral weight transfer by doping increases systematically with the increase of the one-electron bandwidth W .

On the other hand, the Ti-O-Ti bond angle can be decreased as we decrease the ionic radius of the R site. The decrease of the Ti-O-Ti bond angle gives rise to the decrease of the value of W . A systematic change of the optical conductivity spectra was reported on $RTiO_3$ (R =La, Ce, Pr, Nd, Sm, and Gd).⁷ The lowest gaplike feature systematically increases as the ionic radius of the R site decreases, namely, as the value of W decreases. A similar change was also observed on an alloy system, $\text{La}_{1-x}\text{Y}_x\text{TiO}_3$.⁸ These systematic variations of the optical conductivity are interpreted as the successive increase of the Mott-Hubbard gap with the increase of the strength of the U/W ratio. In these materials, however, the system remains an insulator even for the least correlated LaTiO_3 , therefore one cannot study the evolution of the metallic properties under the bandwidth control in this system.

The purpose of this paper is to clarify the evolution of the optical conductivity spectrum in the metallic phase near the Mott transition, as we control the strength of the electron correlation U/W without changing the band filling. A perovskite-type $3d^1$ vanadate CaVO_3 is considered to be a strongly correlated metal close to the Mott transition.^{13,14} We can control the strength of the U/W ratio, by chemical substitution of a Sr ion for a Ca ion of the same valence without varying the nominal $3d$ -electron number per vanadium ion.¹⁵ We report the optical conductivity spectra in this strongly correlated alloy system $\text{Ca}_{1-x}\text{Sr}_x\text{VO}_3$. The effective mass m^* estimated from the optical measurements is shown in Sec. III B. The evolution of the optical conductivity is discussed in Sec. III C.

II. EXPERIMENT

Single crystals of $\text{Ca}_{1-x}\text{Sr}_x\text{VO}_3$ ($x=0, 0.25, 0.5, 1$) were grown by a floating-zone method using an infrared image furnace with double halogen lamps. Details on the preparation of these samples are described in the preceding paper.¹⁴ Since as-grown samples are slightly oxygen deficient; all of the samples were annealed in air at 200 °C for 24 h in order to make the oxygen concentration stoichiometric.^{13,16,17}

Raman-scattering spectra were measured at room temperature in backscattering geometry in the flowing He gas atmosphere using a triple spectrometer system (Jasco TRS-600) equipped with a charge-coupled device (CCD; Photometrics TK512CB) cooled by liquid nitrogen. The samples were excited by the 514.5 nm Ar ion laser line. Polarization of the incident light was taken to be parallel to that of the scattered light.

Optical reflectivity measurements were carried out at room temperature (~ 300 K) in the energy range between 0.05 eV and 40 eV using a Michelson-type Fourier-transform infrared spectrometer (0.05–0.6 eV), a grating monochromator (0.5–5.6 eV), and a Seya-Namioka-type grating for the

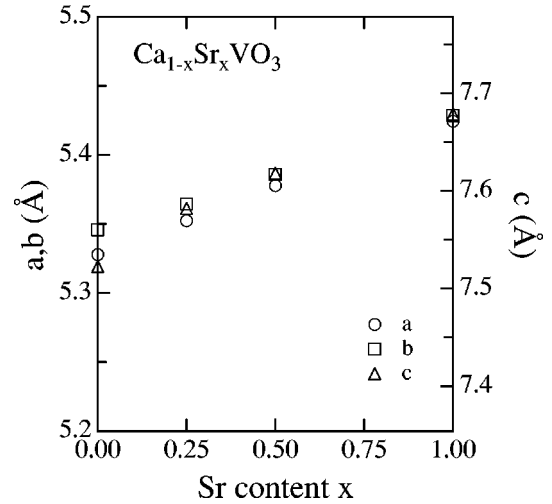


FIG. 1. Lattice constants, a , b , and c of the $\text{Ca}_{1-x}\text{Sr}_x\text{VO}_3$ single crystals plotted against the Sr content x . The data were estimated from powder x-ray diffraction patterns.

synchrotron radiation (5–40 eV) at the beamline BL-11D of Photon Factory, Tsukuba. The surfaces of the samples were mechanically polished with diamond paste for the optical measurements. The absolute reflectivity was determined by referring to the reflectivity of an Al or Ag film which was measured at same optical alignment.

We have calculated a complex dielectric function $\epsilon(\omega) \equiv \epsilon_1(\omega) + i\epsilon_2(\omega)$ by the Kramers-Kronig (K-K) transformation of the measured reflectivity $R(\omega)$, where ω is the photon energy. The real part of the complex optical conductivity $\text{Re}[\tilde{\sigma}(\omega)]$ is related to the imaginary part of the dielectric function $\epsilon_2(\omega)$ by $\text{Re}[\tilde{\sigma}(\omega)] = (\omega/4\pi)\epsilon_2(\omega)$. Since the K-K analysis requires $R(\omega)$ for $0 < \omega < \infty$, two assumptions must be made to extrapolate the observed data beyond the upper and lower bounds of the measurements. In the present study, the reflectivity data were first extrapolated from the lowest measured energy down to $\omega = 0$ with the Hagen-Rubens formula, which is an approximation for $R(\omega)$ of conventional metals. Then, beyond the highest measured energy, the reflectivity data were extrapolated up to $\omega \rightarrow \infty$ with an asymptotic function of ω^{-4} .

III. RESULTS AND DISCUSSION

A. Bandwidth control due to orthorhombic distortion

Powder x-ray diffraction measurements were carried out to characterize the samples and to determine the lattice constants. In Fig. 1, we present the lattice constants, a , b , and c against the Sr content x . The crystal structure of $\text{Ca}_{1-x}\text{Sr}_x\text{VO}_3$ belongs to the perovskite-type structure with orthorhombic distortion (GdFeO₃ type).¹⁸ The amount of the distortion is almost proportional to the amount of the Ca content; i.e., SrVO_3 is a cubic perovskite. However, we assumed the crystal structure of all samples ($0 \leq x \leq 1$) orthorhombic and deduced the lattice constants. The lattice constants increase monotonously with the increase of x , ensuring the appropriate formation of the solid solution over the whole composition range.

Raman-scattering measurements give indirect information about the crystal symmetry, because the appearance of some

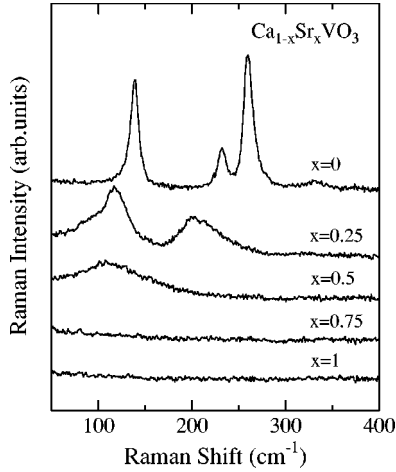


FIG. 2. Raman spectra of $\text{Ca}_{1-x}\text{Sr}_x\text{VO}_3$ at room temperature. Polarization of the incident light was taken to be parallel to that of the scattered light.

Raman-active phonon lines depends crucially on the crystal symmetry of the system. In Fig. 2, we show the Raman spectra of $\text{Ca}_{1-x}\text{Sr}_x\text{VO}_3$ at room temperature in the wave-number range of 80–400 cm^{-1} . In this wave-number range, four Raman active A_g phonon lines are observed in orthorhombic CaVO_3 ($x=0$). The energies of the phonon lines shift to the lower-energy side, and the width of the peaks become broader, as we increase the Sr content x . The Raman-active phonon lines disappear completely in SrVO_3 .

According to the group theory analysis,¹⁹ it is predicted that several Raman-active phonon modes $7A_g + 7B_{1g} + 5B_{2g} + 5B_{3g}$ can exist in the orthorhombically distorted perovskite that belongs to the point-group symmetry of D_{2h} . On the other hand, the cubic perovskite that belongs to the point-group symmetry of O_h is “Raman forbidden,” namely, it has no Raman-active phonon modes. Therefore, the experimental results tell us that the crystal symmetry actually changes from the orthorhombic distorted perovskite (CaVO_3) to the cubic perovskite (SrVO_3). The orthorhombic to cubic transition is considered to occur between $x=0.5$ and 0.75 .

As discussed in the preceding paper,¹⁴ the orthorhombic distortion implies that the V-O-V bond angle is deviated from 180° , i.e., there is an alternately tilting network of the VO_6 octahedra. The V-O-V bond angle of SrVO_3 is 180° same as an ideal perovskite structure, while that of CaVO_3 is $\sim 160^\circ$. The bond angle deviation from 180° reduces the overlap between the neighboring V $3d$ orbital mediated by the O $2p$ orbital. Therefore, the one-electron bandwidth W of V $3d$ band decreases with decreasing the V-O-V bond angle. Accordingly, we can control the value of W by chemical substitution of the Ca^{2+} ion for the Sr^{2+} ion of the same valence without varying the nominal $3d$ -electron number per vanadium ion. Since the electron correlation energy U is almost the same in CaVO_3 and SrVO_3 , we can thus control the strength of the U/W ratio by the chemical substitution. The V-O-V bond angle of CaVO_3 , in addition, is almost equal to that of LaTiO_3 which is a Mott-Hubbard-type insulator, so that it seems reasonable to consider that CaVO_3 is close to the Mott transition. Moreover, there are many other evidences of the strong electron correlation in this system

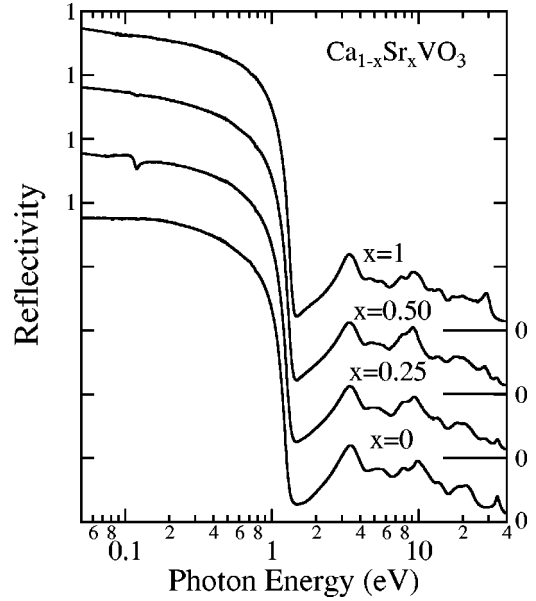


FIG. 3. Reflectivity spectra for the $\text{Ca}_{1-x}\text{Sr}_x\text{VO}_3$ single crystals measured at room temperature. The feature at ~ 0.1 eV for $x=0.25$ is an experimental artifact.

discussed so far.^{13–17} Thus, the $\text{Ca}_{1-x}\text{Sr}_x\text{VO}_3$ system is ideal for the study of the metallic states near the Mott transition.

B. Effective mass

In Fig. 3, we show optical reflectivity spectra of $\text{Ca}_{1-x}\text{Sr}_x\text{VO}_3$ measured at room temperature (~ 300 K), for four single crystals with different x ($x=0, 0.25, 0.50, 1$). The chemical substitution of Sr^{2+} for Ca^{2+} seems to make no remarkable change at the lower-energy region (below ~ 5 eV) in the optical reflectivity spectra. All the samples exhibit high reflectivity from the far-infrared to near-infrared region, and we can recognize a sharp reflectivity edge appearing at ~ 1.3 eV. Since $\text{Ca}_{1-x}\text{Sr}_x\text{VO}_3$ is metallic over the whole composition range, the optical reflectivity is dominated by the signal of conduction electrons in this photon energy region. Systematic spectral changes with x are observed in the energy range of the ultraviolet and vacuum-ultraviolet light. The changes are partly due to the differences in the conduction bands of the Ca^{2+} and Sr^{2+} cations. But this is irrelevant for the discussion of the main subject.

First of all, we will concentrate on the low-energy response of the itinerant carriers. The contribution of the conduction electrons to the complex dielectric function $\epsilon(\omega)$ is well described by the Drude model. According to the generalized Drude model,^{20,21} $\epsilon(\omega)$ is expressed as

$$\epsilon(\omega) = \epsilon_\infty - \frac{4\pi\tilde{\sigma}(\omega)}{i\omega} \equiv \epsilon_\infty - \frac{\omega_p^2(\omega)}{i\omega(\gamma(\omega) - i\omega)}, \quad (1)$$

where ϵ_∞ is the high-energy dielectric constant, which is a high-energy contribution of the interband transitions, $\tilde{\sigma}(\omega)$ is the complex conductivity, $\gamma(\omega)$ is the energy-dependent scattering rate, and $\omega_p(\omega)$ is the plasma frequency. The plasma frequency $\omega_p(\omega)$ is defined as

$$\omega_p^2(\omega) \equiv \frac{4\pi n e^2}{m^*(\omega)},$$

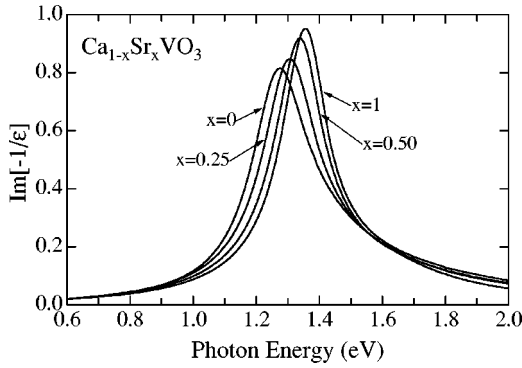


FIG. 4. Energy-loss function $\text{Im}[-1/\epsilon(\omega)]$ obtained by the Kramers-Kronig transformation of the reflectivity data. The data in the photon energy range between 0.6 eV and 2.0 eV are shown to focus on the plasmon peak (around 1.3 eV).

where n is the total density of conduction electrons, and $m^*(\omega)$ is the energy-dependent effective mass.

To begin, let us confine our attention to the plasma frequency. If we assume that the nominal electron number per vanadium ion is exactly 1 for the whole composition range, we can deduce the carrier density n from the unit-cell volume. Then, we can estimate a variation of the effective mass $m^*(\omega)$ from the value of $\omega_p(\omega)$.

The energy-loss function $\text{Im}(-1/\epsilon)$ is obtained by the Kramers-Kronig analysis of the measured reflectivity spectra $R(\omega)$. Provided that $\gamma(\omega)$ and $m^*(\omega)$ do not depend on ω strongly, we can estimate $\omega_p(=\text{const})$ from the energy-loss function, because the energy-loss function peaks at the energy of ω_p^* ($\omega_p^* = \omega_p / \sqrt{\epsilon_\infty}$). Accordingly, we can obtain the energy-independent plasma frequency ω_p from the peak position of the energy-loss function.

In Fig. 4, the spectra of $\text{Im}(-1/\epsilon)$ of $\text{Ca}_{1-x}\text{Sr}_x\text{VO}_3$ are shown in the photon energy range 0.6–2.0 eV to focus on the peak near the reflectivity edge (approximately 1.3 eV). The peak position of the energy-loss function ω_p^* systematically shifts to higher energy with increasing x . At first, we have estimated ω_p^* from the peak energy, and deduced $\omega_p = \sqrt{\epsilon_\infty} \omega_p^*$. If we consider only the response of the conduction electrons, ϵ_∞ is the contribution from the high-energy interband transitions. Since the interband transition appeared above ~ 2.5 eV, the value of ϵ_∞ can be taken from the real part of the dielectric function $\epsilon_1(\omega)$ at around 2.5 eV.²² Since the value of $\epsilon_1(\omega \sim 2.5$ eV) is nearly independent of x , we have used $\epsilon_\infty = 4$ over the whole composition range. Then, we can deduce the value of m^* using the lattice constants and the value of ω_p .

In Fig. 5, the ratios of the deduced effective mass m^* to the bare electron mass m_0 are plotted as a function of the Sr content x . The value of m^*/m_0 systematically increases as varying x from SrVO_3 to CaVO_3 . This carrier-mass enhancement, however, is not so large, even though the system is near the Mott transition. This result is consistent with the value of m^* estimated from the results of the specific-heat measurements.¹⁴

It is instructive to compare the measured low frequency $\tilde{\sigma}(\omega)$ with the simple Drude model, in which $\gamma(\omega)$ and

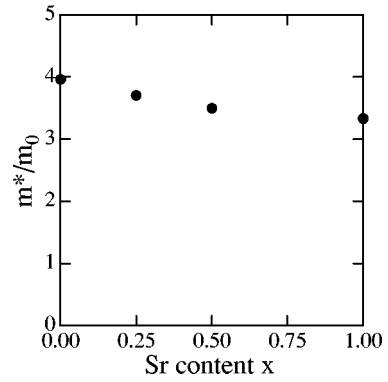


FIG. 5. Effective mass m^* estimated by the plasma frequencies compared with the bare electron mass m_0 . The value of m^*/m_0 systematically increases in going from SrVO_3 ($x=1$) to CaVO_3 ($x=0$).

$m^*(\omega)$ do not depend on ω . According to Eq. (1), the real part of the optical conductivity $\text{Re}[\tilde{\sigma}(\omega)] \equiv \sigma(\omega)$ is given by the formula

$$\sigma(\omega) = \frac{\sigma_{dc}}{1 + \omega^2/\gamma^2},$$

where σ_{dc} is the dc conductivity. The dc conductivity is expressed by the scattering rate γ and the plasma frequency ω_p by the following relation:

$$\sigma_{dc} = \frac{ne^2}{m^* \gamma} = \frac{\omega_p^2}{4\pi\gamma}.$$

Here, we have used the value of σ_{dc} obtained by electric resistivity measurements at room temperature. Then the value of γ can be deduced from the above relation. Figure 6 shows the comparison of the experimentally obtained $\sigma(\omega)$ for CaVO_3 to the optical conductivity calculated by the simple Drude model. As shown in Fig. 6, the contribution to the optical conductivity below ~ 1 eV, which is considered to be a response of the itinerant carriers, is not properly reproduced with the simple Drude model especially above 0.2 eV. As we increase the photon energy, the experimentally obtained $\sigma(\omega)$ deviates from that of the simple Drude

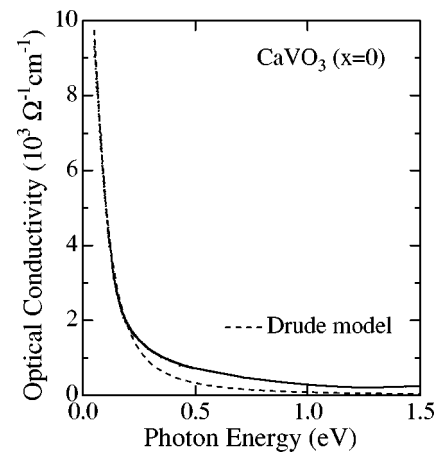


FIG. 6. Comparison between the optical conductivity calculated by the simple Drude model and that of the experiment of CaVO_3 .

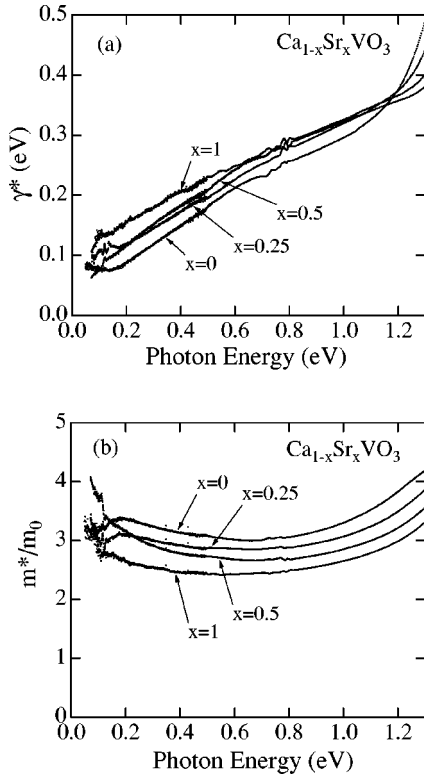


FIG. 7. (a) Energy-dependent scattering rates $\gamma(\omega)$ of $\text{Ca}_{1-x}\text{Sr}_x\text{VO}_3$; (b) effective mass $m^*(\omega)$ of $\text{Ca}_{1-x}\text{Sr}_x\text{VO}_3$. $m^*(\omega)$ is normalized to the bare electron mass m_0 .

model. The observed $\sigma(\omega)$ has a tail decaying slower than the Drude-type ω^{-2} dependence.

We consider that the discrepancy between the simple Drude model and the experimental results is attributed to the energy-dependence of the scattering rate $\gamma(\omega)$ and the effective mass $m^*(\omega)$. The $\gamma(\omega)$ corresponds to the renormalized scattering rate $\tau^{*-1}(\omega)$, which is $\tau^{-1}[m/m^*(\omega)]$. The quantity $\tau(\omega)$ is closer to the microscopic intrinsic quasiparticle lifetime at $T=0$. We can determine $\gamma(\omega)$ and $m^*(\omega)$ from Eq. (1); i.e., when we define $\epsilon(\omega) \equiv \epsilon_1(\omega) + i\epsilon_2(\omega)$,

$$\gamma(\omega) = \frac{\omega\epsilon_2(\omega)}{\epsilon_\infty - \epsilon_1(\omega)},$$

$$m^*(\omega) = \frac{4\pi ne^2}{\omega^2} \text{Re} \left[\frac{1}{\epsilon_\infty - \epsilon(\omega)} \right]$$

$$= \frac{4\pi ne^2}{\omega^2} \frac{\epsilon_\infty - \epsilon_1(\omega)}{[\epsilon_\infty - \epsilon_1(\omega)]^2 + \epsilon_2^2(\omega)}.$$

Figures 7(a) and 7(b) show $\gamma(\omega)$ and $m^*(\omega)$ of $\text{Ca}_{1-x}\text{Sr}_x\text{VO}_3$ as a function of photon energy. In the case of the simple Drude model, the scattering rate γ is provided to be independent on the photon energy. But, in this system, $\gamma(\omega)$ actually increases as we increase the photon energy, as shown in Fig. 7(a).

The energy-dependent scattering rate is generally based on the electron-phonon scattering and the electron-electron scattering. Since an extremely large T^2 dependence of the dc conductivity observed in the $\text{Ca}_{1-x}\text{Sr}_x\text{VO}_3$ system can be well ascribed to the electron-electron scattering,¹⁴ it is reasonable to consider that the electron-electron scattering gov-

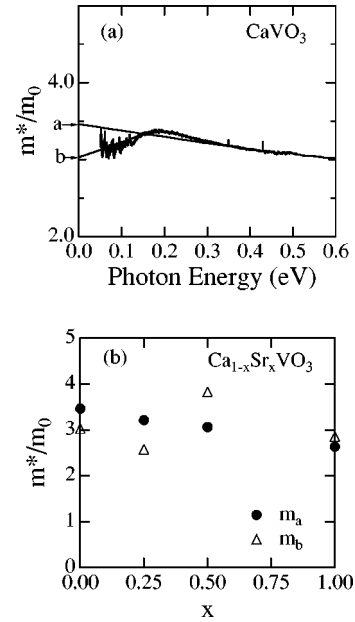


FIG. 8. (a) Energy-dependent effective mass $m^*(\omega)$ of CaVO_3 compared with the bare electron mass. a and b indicate intercepts at which tangential lines drawn from 0.4 eV and 0.15 eV cut the vertical axis, corresponding to the values of m_a and m_b . (b) m_a and m_b are plotted against the Sr content x .

erns the behavior of $\gamma(\omega)$. According to the Fermi liquid theory, the electron-electron scattering rate is proportional to ω^2 . Figure 7(a), however, indicates that $\gamma(\omega)$ looks more proportional to ω rather than ω^2 . On the contrary, since the electron-phonon scattering is proportional to ω^5 up to the Debye frequency, it is necessary to elucidate the scattering process that contributes to $\gamma(\omega)$. This is still an open question.

On the other hand, the energy dependence of $m^*(\omega)$ is not so large. Except for the low-energy region ($\omega < \sim 0.2$ eV), the value of m^*/m_0 increases with the decrease of Sr content x . In the $\text{Sr}_{1-x}\text{La}_x\text{TiO}_3$ system, which is a typical doping system, as one approaches $x=1$, a large energy dependence of m^* as well as a critical enhancement at the low-energy region are observed.² However, in the $\text{Ca}_{1-x}\text{Sr}_x\text{VO}_3$ system, m^* does not exhibit such a critical enhancement with varying x in going from SrVO_3 to CaVO_3 , although there is a difference between the filling control and the bandwidth control.

In the low-energy limit ($\omega=0$), m^* should correspond to the effective mass estimated by the specific-heat measurement. We have interpolated $m^*(\omega)$ down to $\omega=0$ with two kinds of tangential lines drawn from 0.4 eV and 0.15 eV. As shown in Fig. 8(a), the intercepts, at which the two tangential lines from 0.4 eV and 0.15 eV cut the vertical axis, are defined as m_a and m_b . Figure 8(b) indicates the x dependence of the values of m_a and m_b . The value of m_b does not show a systematic behavior, because phonons, randomness, or other extrinsic contributions possibly cause this nonsystematic change. However, the value of m_a increases systematically with decreasing x ; moreover, the values are almost equal to the value of m^* deduced from plasma frequency. We regard m_a as a good measure of m^*/m_0 for this system.

The effective mass estimated from the plasma frequencies

TABLE I. Effective mass m^*/m_0 deduced from the plasma frequencies ω_p and the generalized Drude model (m_a).

x	0	0.25	0.5	1
m^*/m_0 (deduced from ω_p)	3.9	3.7	3.5	3.3
m_a (generalized Drude analysis)	3.5	3.2	3.1	2.7

and the generalized Drude analysis (m_a) appear in Table I. It is expected that we should observe, near the Mott transition, a critical enhancement of the effective mass of the $3d$ conduction electrons. If we substitute the Ca^{2+} ion for the Sr^{2+} ion in the $\text{Ca}_{1-x}\text{Sr}_x\text{VO}_3$ system, the $3d$ bandwidth successively decreases. Then, the value of m^*/m_0 is expected to increase drastically reflecting the change of the U/W ratio. But we have observed that such a large mass enhancement does not actually take place in this system. This is consistent with the result shown in the preceding paper.¹⁴

C. Spectral weight redistribution of $3d$ band

The density of states (DOS) of orthorhombic CaVO_3 and cubic SrVO_3 calculated using the full-potential augmented plane-wave method with the local-density approximation (LDA) are shown in the top part of Fig. 9. The band calculation shows that the DOS near the Fermi level E_F is dominated by the $V 3d$ electrons. The $V 3d$ band crosses the Fermi level, and the DOS below 4 eV is mainly the $O 2p$ band.

In the metallic states, $\sigma(\omega)$ is expected to consist of two basic components: intraband transitions within the $V 3d$ conduction band, i.e., the Drude part extending from $\omega=0$, and interband transitions appearing at much higher energy. The latter is regarded from the calculated DOS as the charge-transfer contribution (an excitation from the $O 2p$ band to the unoccupied part of the $V 3d$ band above E_F). A corre-

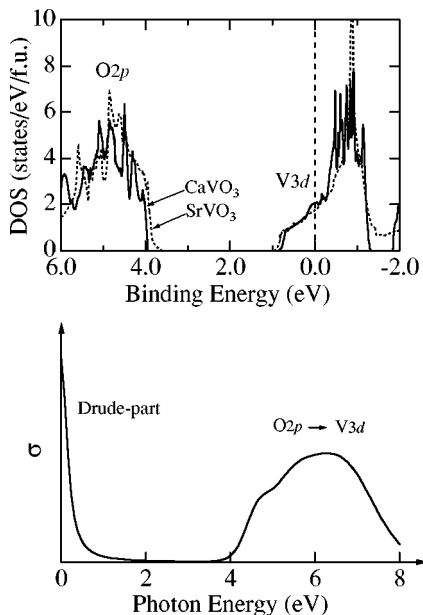


FIG. 9. DOS of CaVO_3 and SrVO_3 obtained by the LDA band calculation (top) and a schematic picture of optical conductivity expected from the calculated DOS (bottom).

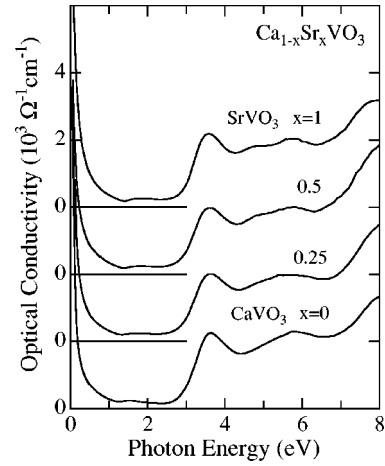


FIG. 10. Optical conductivity spectra of the $\text{Ca}_{1-x}\text{Sr}_x\text{VO}_3$ single crystals ($x=0, 0.25, 0.50, 1$) at room temperature obtained by the Kramers-Kronig transformation of the reflectivity data.

sponding schematic picture of the optical conductivity is shown in the bottom part of Fig. 9. As seen in the picture, the charge-transfer contribution is expected to appear above ~ 4 eV, and the absorption edge of the charge-transfer transition in SrVO_3 is considered to shift slightly to lower energy than that of CaVO_3 , reflecting the shift of the $O 2p$ band.

Based on this picture, let us now look at the experimental results; Fig. 10 shows the real part of the optical conductivity, $\sigma(\omega)$, of the $\text{Ca}_{1-x}\text{Sr}_x\text{VO}_3$ single crystals ($x=0, 0.25, 0.50, 1$). The optical conductivity spectra are different from our naive schematic picture (Fig. 9 bottom); they show the presence of two anomalous features in the intraband transition part below 4 eV besides the Drude-like absorption (discussed above): a small peak that appears at ~ 1.7 eV and a large peak at ~ 3.5 eV. It must be noted that the two peaklike structures below 4 eV have no naive origin as far as we can infer from the calculated DOS (Fig. 9). This large spectral weight redistribution is generally believed to be a manifestation of the strong electron correlation in this system.

Figure 11 shows a comparison of the optical conductivity spectra of CaVO_3 to those of other perovskite oxides, $\text{Sr}_{0.95}\text{La}_{0.05}\text{TiO}_3$ (lightly doped $3d^{0.05}$ metal),²³ and YTiO_3 ($3d^1$ insulator) reported by Okimoto *et al.*⁸ In the optical conductivity of $\text{Sr}_{0.95}\text{La}_{0.05}\text{TiO}_3$, the most prominent low-energy feature, that distinctly rises around 4 eV, can be interpreted as originating in a transition from the $O 2p$ band to the $\text{Ti } 3d$ band, which corresponds to the optical gap of the parent insulator SrTiO_3 .²⁴ The doped $3d$ electrons contribute to $\sigma(\omega)$ with a small spectral weight extending from $\omega=0$. On the other hand, YTiO_3 is considered to be a Mott-Hubbard insulator. Two electronic gaplike features are observed around 1 eV and 4 eV. These features have been, respectively, interpreted as originating in excitations through the Mott-Hubbard gap, namely, from the lower-Hubbard band (LHB) to the upper-Hubbard band (UHB), and as excitations through the charge-transfer gap, i.e., from the $O 2p$ band to the UHB.^{8,25} Recently, Bouarab, Vega, and Khan have reported interband optical conductivities obtained by the energy-bands calculation of the YMO_3 ($M=\text{Ti-Cu}$) system with a local spin-density approximation.²⁶ Their calculated results of interband optical conductivity in YTiO_3 is

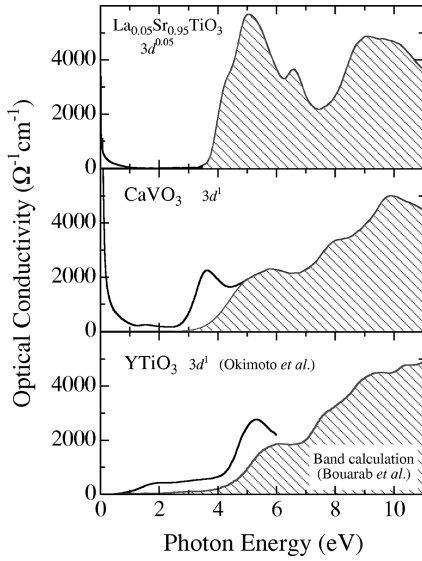


FIG. 11. Comparison of the optical conductivity spectra of CaVO_3 to those of other perovskite oxides, $\text{Sr}_{0.95}\text{La}_{0.05}\text{TiO}_3$ (lightly doped $3d^0$ metal) (Ref. 23), and YTiO_3 ($3d^1$ insulator) reported by Okimoto *et al.* (Ref. 8). Shaded portions correspond to the interband transition, and remaining white portions correspond solely to the intraband transitions within the V $3d$ band.

shown in the bottom of Fig. 11 as a shaded portion. We find out from this comparison that the peak at approximately 5 eV cannot be explained by the transition between the O $2p$ band and the Ti $3d$ band alone.

In CaVO_3 , photoemission spectroscopy^{15,27} has revealed that the O $2p$ band is located at a binding energy that is almost the same as that of metallic $\text{Sr}_{0.95}\text{La}_{0.05}\text{TiO}_3$; hence, the absorption edge of the charge-transfer excitation of CaVO_3 should be approximately equal to that of $\text{Sr}_{0.95}\text{La}_{0.05}\text{TiO}_3$. Therefore, it is reasonable to consider that the shaded portions of $\sigma(\omega)$ in Fig. 11 correspond to the charge-transfer type transitions as well as the other interband transitions with much higher energies, on the analogy of the band calculation in YTiO_3 .²⁶ Accordingly, the remaining white portions correspond solely to the intraband transition within the V $3d$ band.

In order to focus on the spectral weight of the optical conductivity arising from intra- $3d$ -band transitions, we have subtracted the shaded portion in the middle of Fig. 11 as backgrounds, assuming an appropriate function of $(\omega - \Delta)^{3/2}$, where Δ has been obtained by fitting the lower-energy tail of the O $2p$ band in photoemission spectroscopy spectra of $\text{Ca}_{1-x}\text{Sr}_x\text{VO}_3$ single crystals.²⁸

A quantitative measure of the spectral weight has been obtained by deducing the effective electron number per vanadium ion defined by the following relation:

$$N_{\text{eff}}(\omega) \equiv \frac{2mV}{\pi e^2} \int_0^\omega \sigma(\omega') d\omega',$$

where e is the bare electronic charge and m is the bare band mass of a noninteracting Bloch electron in the conduction band. V is the cell volume for one formula unit (one V atom in this system). The significance of N_{eff} will be appreciated by considering the sum rule of the conductivity

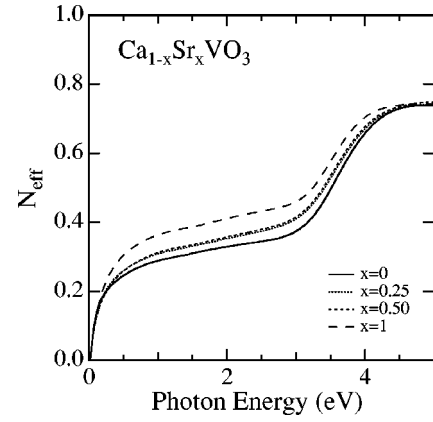


FIG. 12. Effective electron number per vanadium atom N_{eff} obtained after subtracting the higher-energy background (Fig. 11).

$$\int_0^\infty \sigma(\omega) d\omega = \frac{\pi N e^2}{2mV}$$

where $N \equiv N_{\text{eff}}(\infty)$ corresponds to the total number of electrons in the unit formula. That is, $N_{\text{eff}}(\omega)$ is proportional to the number of electrons involved in the optical excitations up to ω . In Fig. 12, we show N_{eff} of the $\text{Ca}_{1-x}\text{Sr}_x\text{VO}_3$ system, after subtracting the higher-energy background. Since, in Fig. 12, we have assumed $m = m_0$, where m_0 is the bare electronic mass, the total number $N \equiv N_{\text{eff}}(\omega = \infty) \approx N_{\text{eff}}(\omega = 5 \text{ eV})$ result is smaller than 1, reflecting the difference between m and m_0 ($m > m_0$). If we rather use the value m obtained from LDA, $m \sim 1.5m_0$ for the V $3d$ band, we find $N_{\text{eff}}(5 \text{ eV}) \approx 1$. Thus, we conclude that the assumed background (shaded area in Fig. 11) is reasonable to deduce the intrinsic contributions of the interband transition.

The initial steep rise of N_{eff} is due to the Drude-like contributions extending from $\omega = 0$. The Drude-like contribution can be distinguished below ~ 1.5 eV, where N_{eff} exhibits a flat region. Therefore, N_{eff} at ~ 1.5 eV is considered to be a good measure for the effective mass of the carries. The values of m^*/m_0 estimated from $N_{\text{eff}}(\omega = 1.5 \text{ eV})$ are 3.1(6), 3.0(5), 3.0, 2.7 for $x = 0, 0.25, 0.50, 1$, which are almost equivalent to the values of m^*/m_0 discussed in Sec. III B.

Figure 13 shows the optical conductivity spectra $\sigma(\omega)$ of the $\text{Ca}_{1-x}\text{Sr}_x\text{VO}_3$ single crystals ($x = 0, 0.25, 0.50, 1$) in the photon energy range of 0–5 eV. The high-energy background corresponding to the interband transition is subtracted. As discussed above, $\sigma(\omega)$ ($0 \leq \omega \leq 5 \text{ eV}$) reflects only the intraband transition of the V $3d$ electrons. In the spectrum, there is a small feature at ~ 1.7 eV, which we call peak A [Fig. 13(a)] and also a large feature at ~ 3.5 eV, which we call peak B [Fig. 13(b)]. With the increase of x , the excitation energy of peak B shifts slightly to lower energy, and its spectral weight decreases; whereas, the excitation energy of peak A shifts to higher energy, and its spectral weight increases. In addition, the width of peak A broadens with the increase of x . Figure 14 shows the excitation energy, the full width at half-maximum, and the spectral weight of peaks A and B as functions of x .²⁹

In the valence-band photoemission spectra of the $\text{Ca}_{1-x}\text{Sr}_x\text{VO}_3$ system, two features have been observed: one is a peak at ~ 1.5 eV below E_F and the other is the emission

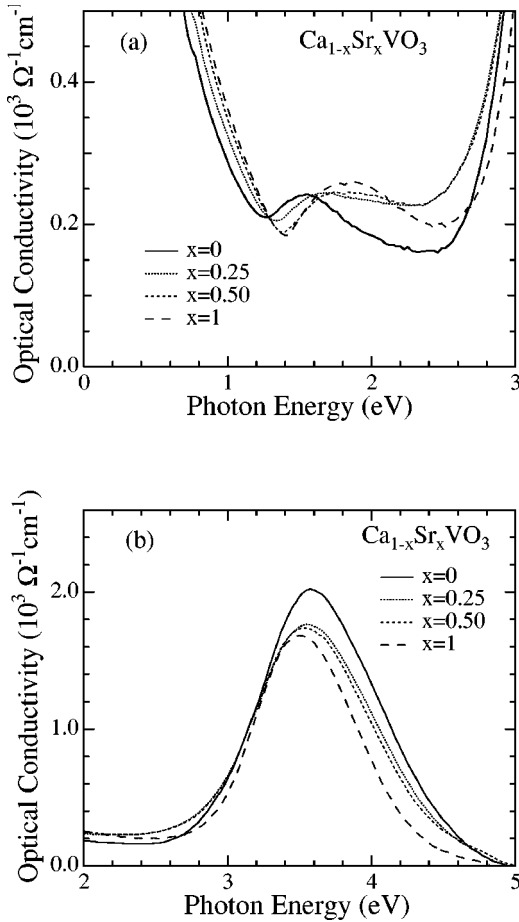


FIG. 13. Optical conductivity spectra of the $\text{Ca}_{1-x}\text{Sr}_x\text{VO}_3$ in the photon energy range of 0–5 eV. The high-energy background corresponding to the interband transition is subtracted. (a) a small peak at ~ 1.7 eV denoted as peak A in the text. (b) a large peak at ~ 3.5 eV denoted as peak B in the text.

from a broad quasiparticle band that lies on E_F .^{15,27} The former is assigned to an incoherent emission associated with the formation of the lower Hubbard band and the latter corresponds to a renormalized 3d band at E_F . Inoue *et al.* reported that, upon increasing the strength of U/W in the $\text{Ca}_{1-x}\text{Sr}_x\text{VO}_3$ system, the spectral weight is systematically transferred from the quasiparticle band to the incoherent part.¹⁵ In the inverse-photoemission spectra of CaVO_3 and SrVO_3 , Morikawa *et al.* have found a prominent peak at 2.5–3 eV above E_F and a shoulder within around 1 eV of E_F .²⁷ These features have been also assigned to the incoherent and coherent parts of the spectral function of the V 3d electron. These results lead us into consideration that the two features (peaks A and B) observed in the optical conductivity spectra should originate in possible combinations of the transitions among the incoherent and coherent features of V 3d electron around the Fermi level.

The experimental results of the optical conductivity can be compared to the theoretical prediction obtained by the self-consistent local-impurity approximation of the infinite-dimension Hubbard model.¹² The theory seems to give us a clue to understand the origin of the two features: peaks A and B. According to the prediction, the optical response is composed of basically three contributions except for the Drude part: a broad part centered at a frequency $\omega = U$, a few nar-

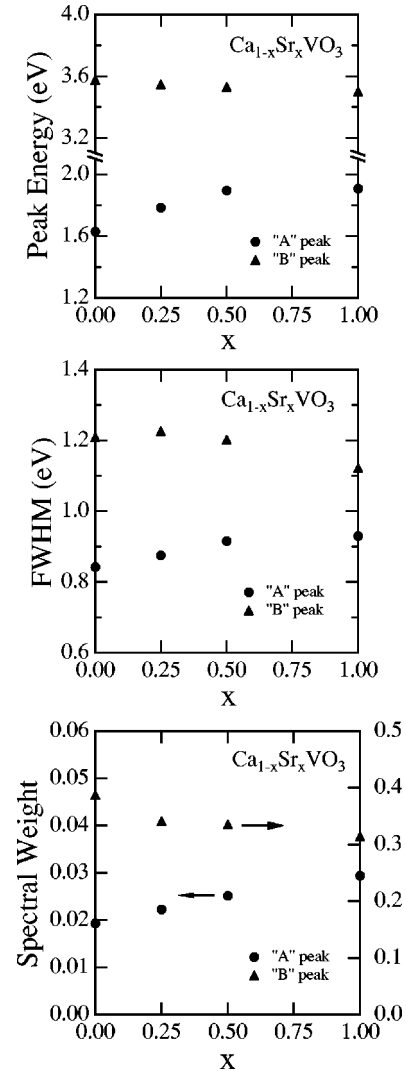


FIG. 14. Excitation energy, full width at half-maximum (FWHM), and spectral weight of peaks A and B plotted as functions of x .

row features near $\omega = U/2$, and an “anomalous” part that is present in the range $\omega = 0-1$ eV, approximately. The contribution at U corresponds to direct excitations between the Hubbard bands, the features at $U/2$ correspond to excitations from the LHB to the empty part of the quasiparticle band and from the filled part of the quasiparticle band to the UHB, and finally, the anomalous part corresponds to excitations from the filled to the empty part of the quasiparticle band. In our previous paper,³⁰ we analyzed the spectrum of CaVO_3 in the light of these predictions. The parameters U and W , which were used in the model calculation, were taken from the results of photoemission spectroscopy.³⁰ Although it was expected that the parameter W would systematically change with composition, we chose to vary U for the sake of simplicity, given that fits of equivalent quality could be obtained for the photoemission spectra. In CaVO_3 , which has the narrowest 3d band in the $\text{Ca}_{1-x}\text{Sr}_x\text{VO}_3$ system, peaks A and B have been well described by the features at $U/2$ and U , respectively, so that the infinite-dimensional Hubbard model seems to reproduce the experimentally obtained optical conductivity reasonably well.³⁰

We find that our experiment gives results as summarized

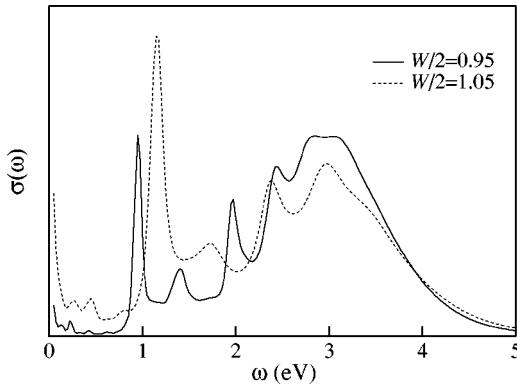


FIG. 15. Calculated optical conductivity by IPT for the parameters $U=3$ eV and W indicated in the figure.

in Fig. 14: with the increase of x , the peak energy of peak B shifts slightly to the lower-energy side and its spectral weight gradually increases. The spectral weight of peak A increases with x . Peak A , however, shifts slightly to higher energy. We would now like to emphasize an important point. Our present systematic study of the $\text{Ca}_{1-x}\text{Sr}_x\text{VO}_3$ compound gives conclusive evidence that we can tune the bandwidth of the system by controlling x . The position of peak B gives a direct measure of the value of U , and the fact that it remains almost a constant is clear evidence that the ratio U/W is controlled by a change of the bandwidth W . This situation is in sharp contrast to our previous analysis³⁰ based on photoemission data, which did not allow us to resolve which parameter was actually controlling the U/W ratio. A crucial ingredient that makes the study of the optical response so valuable for this analysis is that, unlike photoemission, it probes also the unoccupied part of the spectra; therefore, it is sensitive to the relative position of the Hubbard bands.

In order to gain some further insight into the qualitative behavior of the systematic evolution of our experimental data, we have used our initial estimates for U and W as input parameters in a calculation of the optical response of the Hubbard model and changed the value of W instead of U . We shall consider the model within the dynamical mean-field theory, which becomes exact in the limit of large lattice connectivity (or large dimensionality). For convenience we have computed the optical response using the iterated perturbation theory (IPT) method, which allows for a simple evaluation of this quantity at $T=0$ and near the Mott-Hubbard transition.^{31,32}

In Fig. 15 we show the theoretical prediction using the value of $U=3$ eV for the local repulsion and for the half-bandwidth $W/2=1.05$ and 0.95 eV for SrVO_3 and CaVO_3 , respectively. Note that the spectra do not display the Drude contribution as it corresponds to a δ function at $\omega=0$ since our model does not contain disorder and the calculation is performed at $T=0$. The particular line shape that we obtain is originated in the behavior of the spectral density of states that is obtained within the IPT method as shown in Fig. 16. We should point out that while the details of the line shape may not be correctly given by this method, the main distribution of the spectral weight of the various contributions and their systematic evolution are very reliably captured.¹²

We observe that the theoretical results for the systematic dependence of the various contributions to the optical re-

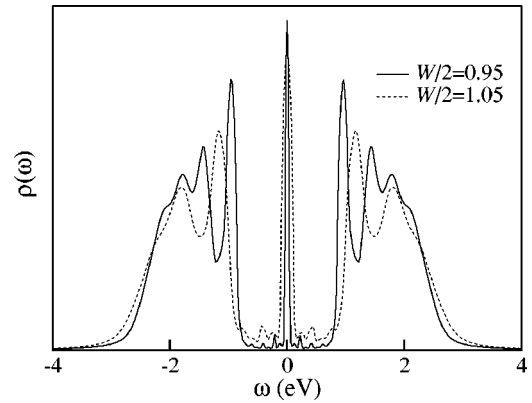


FIG. 16. Theoretical spectral density of states obtained by IPT at $T=0$ for the parameters $U=3$ eV and W indicated in the figure.

sponse by controlling the value of W are in better qualitative agreement with the experimental data of Fig. 14 than the previous calculation where we changed the value of U . One of the most notable improvements consists of the fact that the unexpected systematic evolution of the feature at $U/2$, which shifts upward with increasing W , is captured very well qualitatively. This peculiar effect can be interpreted as a ‘‘band repulsion’’ between the Hubbard band and the quasiparticle band. As we increase W , the latter becomes broader and ‘‘pushes’’ the Hubbard band further out.

However, there are still some discrepancies. Such a large spectral weight redistribution is predicted to be concomitant with a large effective mass in the mean-field treatment of the Hubbard model.^{12,33} This is, however, inconsistent with the observed effective mass in this system. Moreover, in the optical conductivity spectra, there is apparently a notable discrepancy with respect to the relative spectral weight of peak A to peak B . It is remarkably suppressed in the experimental data, compared with the theoretical data.

Other discrepancies between some experimental results and the prediction of the mean-field approach for the electron correlation were also reported in the photoemission spectroscopy measurements in this system.^{15,27} In the mean-field Fermi liquid approach, the renormalized quasiparticle band at E_F should be narrowed with increasing the value of U/W ,^{12,33} but, in those experiments, the quasiparticle bandwidth remains broad, even if the system approaches to the Mott transition. Since peak A has been assigned to the transitions associated with the quasiparticle band, the conspicuous suppression in spectral intensity of peak A reflects the broadness of the quasiparticle band. The broad quasiparticle band also accounts for the lack of the strong mass enhancement in this system.

As discussed in the preceding paper,¹⁴ the momentum-dependent self-energy becomes significant near the Mott transition, resulting in a reduction of the mass enhancement. Although our measurement cannot clarify the validity of introducing a momentum-dependent self-energy, we conclude that there must be other interactions not present in the mean-field treatment of the electron correlation in the metallic regime close to the Mott transition.

Finally, the presence of the anomalous contribution at low frequencies that extends down to $\omega=0$ in the theoretical data sheds a different light for the interpretation of the Drude-like response discussed in Sec. III B. It may be possible to say

that the deviation from the simple Drude model would be partly due to this anomalous contribution. The origin of this effect is again traced to the presence of the incoherent contribution coming from the low energy tails of the Hubbard bands that is observed in the theoretical density of states. However, it is experimentally very difficult to disentangle unambiguously the contribution of the coherent optical response of carriers and that of the incoherent process in optical conductivity, so this issue remains an open question.

IV. CONCLUSIONS

This study has aimed at elucidating the electronic structure of the correlated metallic vanadate by means of optical spectroscopy measurements. We have synthesized the $\text{Ca}_{1-x}\text{Sr}_x\text{VO}_3$ system to control solely the $3d$ bandwidth without varying the band filling.

We have found that the low-energy contribution to the optical conductivity spectra cannot be reproduced by the simple Drude model with the energy-independent scattering rate and effective mass. The energy-dependent $\gamma(\omega)$ determined by the generalized Drude model shows relatively

large energy dependence. However, $\gamma(\omega)$ is proportional to ω rather than that of the electron-electron scattering ω^2 .

The effective mass of the V $3d$ electron has been evaluated from the plasma frequency. The value of m^*/m_0 gradually increases with decreasing bandwidth W . However, no symptom of the critical mass enhancement has been observed, even though the system is close to the Mott transition.

We observed two anomalous peaks in the optical conductivity spectra around 1.7 eV and 3.5 eV. These features can be assigned to the possible combinations of transitions between the incoherent and coherent bands of quasiparticles around the Fermi level. This large spectral weight redistribution substantiates the strong electron correlation in this system, which is, however, not concomitant with a large effective-mass enhancement.

ACKNOWLEDGMENTS

We would like to thank the staff of the Photon Factory for its technical support. We also thank Y. Nishihara and F. Iga for their helpful suggestions and experimental support.

*Author to whom correspondence should be addressed. Present address: Electrotechnical Laboratory, Tsukuba 305-8568, Japan. Electronic address: INOUE@ETL.GO.JP

¹N. F. Mott, *Metal-Insulator Transitions* (Taylor and Francis, London, 1974).

²Y. Fujishima, Y. Tokura, T. Arima, and S. Uchida, *Phys. Rev. B* **46**, 11 167 (1992).

³Y. Taguchi, Y. Tokura, T. Arima, and F. Inaba, *Phys. Rev. B* **48**, 511 (1993).

⁴M. Kasuya, Y. Tokura, T. Arima, H. Eisaki, and S. Uchida, *Phys. Rev. B* **47**, 6197 (1993).

⁵D. A. Crandles, T. Timusk, J. D. Garrett, and J. E. Greedan, *Phys. Rev. B* **49**, 16 207 (1994).

⁶T. Katsufuji, Y. Okimoto, and Y. Tokura, *Phys. Rev. Lett.* **75**, 3497 (1995).

⁷D. A. Crandles, T. Timusk, and J. E. Greedan, *Phys. Rev. B* **44**, 13 250 (1991); D. A. Crandles, T. Timusk, J. D. Garrett, and J. E. Greedan, *Physica C* **201**, 407 (1992).

⁸Y. Okimoto, T. Katsufuji, Y. Okada, T. Arima, and Y. Tokura, *Phys. Rev. B* **51**, 9581 (1995).

⁹G. A. Thomas, D. H. Rapkine, S. A. Carter, A. J. Millis, T. F. Rosenbaum, P. Metcalf, and J. M. Honig, *Phys. Rev. Lett.* **73**, 1529 (1994); G. A. Thomas, D. H. Rapkine, S. A. Carter, T. F. Rosenbaum, P. Metcalf, and D. F. Honig, *J. Low Temp. Phys.* **95**, 33 (1994).

¹⁰M. J. Rozenberg, G. Kotliar, H. Kajueter, G. A. Thomas, D. H. Rapkine, J. M. Honig, and P. Metcalf, *Phys. Rev. Lett.* **75**, 105 (1995).

¹¹J. Zaanen, G. A. Sawatzky, and J. W. Allen, *Phys. Rev. Lett.* **55**, 418 (1985).

¹²A. Georges, G. Kotliar, W. Krauth, and M. J. Rozenberg, *Rev. Mod. Phys.* **68**, 13 (1996).

¹³I. H. Inoue, K. Morikawa, H. Fukuchi, T. Tsujii, F. Iga, and Y. Nishihara, *Jpn. J. Appl. Phys., Part 1* **32**, 451 (1993).

¹⁴I. H. Inoue, O. Goto, H. Makino, N. E. Hussey, and M. Ishikawa, preceding paper, *Phys. Rev. B* **58**, 4372 (1998).

¹⁵I. H. Inoue, I. Hase, Y. Aiura, A. Fujimori, Y. Haruyama, T.

Maruyama, and Y. Nishihara, *Phys. Rev. Lett.* **74**, 2539 (1995).

¹⁶A. Fukushima, F. Iga, I. H. Inoue, K. Murata, and Y. Nishihara, *J. Phys. Soc. Jpn.* **63**, 409 (1994).

¹⁷N. Shirakawa, K. Murata, H. Maikino, F. Iga, and Y. Nishihara, *J. Phys. Soc. Jpn.* **64**, 4824 (1995).

¹⁸B. L. Chamberland and P. S. Danielson, *J. Solid State Chem.* **3**, 243 (1971).

¹⁹M. Couzi and P. V. Huong, *J. Chim. Phys. Phys.-Chim. Biol.* **69**, 1339 (1972).

²⁰J. W. Allen and J. C. Mikkelsen, *Phys. Rev. B* **15**, 2952 (1977).

²¹B. C. Webb, A. J. Sievers, and T. Mihalisin, *Phys. Rev. Lett.* **57**, 1951 (1986).

²²In fact, we should take into account a small contribution of a peak around 1.7 eV in the $\epsilon_1(\omega)$ spectra. The peak corresponds to the A peak in the optical conductivity. But here, we have disregarded the small peak.

²³H. Makino *et al.* (unpublished).

²⁴M. Cardona, *Phys. Rev.* **140**, A651 (1965).

²⁵T. Arima, Y. Tokura, and J. B. Torrance, *Phys. Rev. B* **48**, 17 006 (1993).

²⁶S. Bouarab, A. Vega, and M. A. Khan, *J. Phys.: Condens. Matter* **9**, 6267 (1997).

²⁷K. Morikawa, T. Mizokawa, K. Kobayashi, A. Fujimori, H. Eisaki, S. Uchida, F. Iga, and Y. Nishihara, *Phys. Rev. B* **52**, 13 711 (1995).

²⁸I. H. Inoue, H. Makino, I. Hase, Y. Aiura, Y. Haruyama, and Y. Nishihara, *Physica B* **230-232**, 780 (1997).

²⁹We have divided peaks A and B by fitting the $\epsilon_2(\omega)$ data with two Gaussians. And the spectral weight is defined as an amount of the contributions to $N_{\text{eff}}(\omega)$ from peaks A and B.

³⁰M. J. Rozenberg, I. H. Inoue, H. Makino, F. Iga, and Y. Nishihara, *Phys. Rev. Lett.* **76**, 4781 (1996).

³¹A. Georges and G. Kotliar, *Phys. Rev. B* **45**, 6479 (1992).

³²X. Y. Zhang, M. J. Rozenberg, and G. Kotliar, *Phys. Rev. Lett.* **70**, 1666 (1993).

³³W. F. Brinkman and T. M. Rice, *Phys. Rev. B* **2**, 4302 (1970).